Article:

Wade, A, Beadling, AR orcid.org/0000-0001-5501-0140, Neville, A et al. (4 more authors) (2020) Geometric Variations of Modular Head-Stem Taper Junctions of Total Hip Replacements. Medical Engineering & Physics, 83. pp. 34-47. ISSN 1350-4533

https://doi.org/10.1016/j.medengphy.2020.07.017

Title

Geometric Variations of Modular Head-Stem Taper Junctions of Total Hip Replacements

Authors

A. Wade[a*], A. R. Beadling[a], A. Neville[a], D. De Villiers[b], C. J. Cullum[b], S. Collins[b], and M. G. Bryant[a]

[a] University of Leeds, School of Mechanical Engineering, Institute of Functional Surfaces, Leeds, UK;

[b] MatOrtho Ltd, Mole Business Park, Randalls Rd, Surrey, UK;

[*]Corresponding author, email: mn13aw@leeds.ac.uk

Abstract

Taper degradation in Total Hip Replacements (THR) has been identified as a clinical concern, and the degradation occurring at these interfaces has received increased interest in recent years. Wear and corrosion products produced at the taper junction are associated with adverse local tissue responses, leading to early failure and revision surgery. Retrieval and in-vitro studies have found that variations in taper design affect degradation. However, there is a lack of consistent understanding within the literature of what makes a good taper interface. Previous studies assessed different design variations using their global parameters assuming a perfect cone such as: taper length, cone angle and diameters. This study assessed geometrical variations of as-manufactured head and stem tapers and any local deviations from their geometry. The purpose of this study was to provide a greater insight into possible engagement, a key performance influencing parameter predicted by Morse taper connection theory. This was achieved by taking measurements of twelve different commercially available male tapers and six female tapers using a coordinate measurement machine (CMM). The results suggested that engagement is specific to a particular head-stem couple. This is subject to both their micro-scale deviations, superimposed on their macro-scale differences. Differences in cone angles between female and male tapers from the same manufacturer was found to create a predominately proximal contact. However, distally mismatched couples are present in some metal-on-metal head-stem couples. On a local scale, different deviation patterns were observed from the geometry which appeared to be linked to the manufacturing process. Future work will look at using this measurement methodology to fully characterise an optimal modular taper junction for a THR prosthesis.

Keywords/Phrases

Taper, Geometry, Biotribocorrosion, Taper Interface, Modular Hip Prostheses

1. Introduction

Modularity of the femoral component in Total Hip Replacements (THR) is achieved by incorporating a Morse-type taper at the head-stem connection [1]. It allows alternative head materials with varying sizes and offsets to be used to balance soft tissues in order restore the natural gait [2,3]. Modularity also offers the ability to retain well fixed femoral stems while replacing the femoral head reducing the risk of morbidity, bone loss and soft tissue damage during revision surgery [4]. Exchanging the femoral head while retaining the stem during revision surgery has been recorded to occur in around 45 % of primary revision surgeries in Sweden, according to the Swedish Joint Registry [5]. The 15th annual joint registry for England, Wales, Northern Ireland and Isle of Man (NJR) [6] indicates that at least 630,000 THR implanted between 2003 and 2017 included head-stem modularity. However, moving from a mono-block to a modular design has meant fluid ingress and micro-motion at the interface, leading to a complex degradation mechanism between fretting and corrosion (i.e. fretting-corrosion) [7–9]. Gilbert et al.[8] investigated degradation due to head-stem modularity coining the term Mechanically Assisted Crevice Corrosion (MACC) to describe the mechanical and chemical degradation mechanisms and any interdependence they may have. Wear and corrosion products at the taper junction are associated with adverse local tissue reactions commonly presented in patients as pain followed by instability [10–13]. Fretting-corrosion at the head-stem junction can also present systemic implications, and in some cases go on to cause catastrophic implant failure such as neck fracture or head dislocation due to excessive material loss [2,11,14,15]. The NJR [6] found that of all primary hip replacements, 2.8 % required revision and of that, 17 % were due to adverse soft tissue reaction to particle debris; where the head-stem taper junction is a possible generation source. Taper degradation is a clinical concern and has been received increasing interest in recent years [11,15–17]. This was highlighted by a recent retrieval study conducted by Ridon et al. [18] that compared matched cohorts of metal-on-metal (MoM) THR with resurfacing (no modular femoral stem). They found that almost 30 % of the THR cohort underwent revision due to adverse reactions to metal debris compared to 0 % for the resurfacing cohort, highlighting that the head-stem interface would appear to be a prominent interface for metal ion release. Whilst there has been a dramatic decrease in the use of MoM THR, which now make up only around 4 % of implanted, taper degradation is still a clinical concern with evidence of degradation occurring in all bearing combinations [6,13,16,17,19,20].

Morse tapers were originally designed to allow machine parts such as drill bits and cutting tools in milling machines to be changed quickly without compromising torque transmission [1]. This is achieved by an interference fit between male and female conical surfaces allowing torque transmission under a simple compressive force along the taper length. The original Morse taper achieved a sufficient interference fit by designing the two interfaces to be highly conforming, smooth, hard (usually case-hardened steel), long and with a slight taper angle [21–23]. These design features provide a sufficient compressive fit over the whole mating taper surface to resist shear stress from applied torque. Hardening is undertaken for a number of reasons including: to increase cylindrical accuracy, stiffness and to reduce damage due to handling and fretting from mismatched mating surfaces. Absolute conformity is hard to achieve and so tapers have commonly been designed to relieve the contact at the centre, for a good fit without shaking due to contact at either end [22]. It was also originally advised not to impact tapers, but to use a press to ensure alignment and equal strain or distortion for use in lathes [21].

Head-stem tapers used in THR on the other hand are much shorter with a higher taper rate (i.e. shorter with a greater taper angle), often presenting a threaded finish and a level of angular mismatch (i.e. the difference in cone angle between the female and male taper, see Figure 1) in order to create specific contact regions [1,24]. Additionally, the biomechanical loading profile of the head-stem taper in-vivo is complex with a cyclic nature, very different from that experienced in Morse tapers [25]. Morse tapers were designed to transmit high torques under a dominant compressive axial load (i.e. two axes) [1]. The sort of mechanical loads experienced at the taper junction are complex and include loading is six axes [26,27]. These are dynamic loads and can exceed body weight by almost a factor of four [25]. The complex biomechanical loading facilitates micro-motions and fluid ingress with abundant electrochemically active species for fretting-corrosion [8]. Degradation of the taper junction in THR has been found to vary with different designs parameters including: surface roughness, diameters, angular mismatch, length and flexural rigidity [9,28–35]. However, links to clinical performance are often limited to high level descriptions such as short and rough or long and smooth [32,36].

Engagement of the two conical surfaces has been historically determined by differences in the geometrical form of the male and female taper assuming an ideal cone and deviations from that geometry. This is usually parametrised by angular mismatch, taper length and surface roughness (see Figure 1) [31,33–35,37,38]. However, just looking at the geometry assuming an ideal cone and surface topography provides limited insight into possible engagement for further performance assessment. Witt et al. [39], investigated the engagement of unique head-stem couples by using a gold coating on the male taper, quantifying the removal of this film upon engagement. It was found that engagement of the two surfaces was inconsistently distributed. This raises questions about the conformity of the interface and/or about the impactions process being self-aligning even under quasi-static loading.

This study assessed geometrical variations of as-manufactured head and stem tapers and any local deviations from their geometry, giving a greater insight into possible engagement. Outputs from this study will be used in future work to allow a more descriptive link between taper design and clinical performance. This was achieved by taking precise geometric measurements of clinically available male and female tapers using a coordinate measurement machine (CMM) with development of bespoke analysis algorithms.

2. Materials and Methods

Measurements were taken using a coordinate measurement machine (CMM, Legex 322,Mitutoyo, Japan) accurate to 0.28 µm. The study included twelve different commercially available male tapers and six female tapers (see Table 1). Two of the ten male tapers (MT4 and MT5) were manufactured from simplified spigots coupons, while all the others were full femoral stem. This meant that MT4 and MT5 where clinical '12/14' tapers manufactured from 14 mm diameter bar stock. Manufacturer and product information was kept anonymous for commercial reasons.

Table 1 Details of samples measured using CMM, where 'n' corresponds to the number of different samples. NB 'Spigot' indicates a spigot coupon as opposed to a full stem and rough indicates a visibly 'threaded' type finish.

Male Taper (MT)/Female Taper (FT)	Manufacturer	Type	Rough (Yes/No)	Collared (Yes/No)	Material	n
MT 1	A	12/14	Yes	Yes	CoCrMo	2
MT 2	A	12/14	Yes	No	CoCrMo	3
MT 3	A	12/14	Yes	No	Ti6Al7Nb	1
MT 4	B	12/14 Spigot	Yes	No	CoCrMo	3
MT 5	B	12/14 Spigot	Yes	No	Titanium Alloy	6
MT 6	B	12/14	Yes	No	CoCrMo	1
MT 7	C	12/14	Yes	No	Stainless Steel	8
MT 8	C	10/12	No	No	CoCrMo	8
MT 9	D	12/14	No	No	CoCrMo	1
MT 10	E	Type 1	No	Yes	CoCrMo	1
MT 11	C	12/14	Yes	No	Titanium Alloy	3
MT 12	C	12/14	Yes	Yes	Titanium Alloy	3
FT 1	A	12/14	-	-	CoCrMo	1
FT 2	A	12/14	-	-	CoCrMo	1
FT 3	B	12/14	-	-	CoCrMo	2
FT 4	B	12/14	-	-	Zirconia Toughened Aluminium Oxide	1
FT 5	C	12/14	-	-	CoCrMo	4
FT 6	C	12/14	-	-	CoCrMo	2

The taper surface was scanned using a 1.5 mm diameter ruby with stylus that was 30 mm long. The same measurement strategy was used for both male and female tapers. The flat proximal end of the tapers was used to create the x-y plane in which the origin lay at the centre, as shown in Figure 1a and b. The traces consisted of 32 equally spaced vertical traces along the length of the longitudinal axis of the taper (z-axis) and circumferential traces at 0.5 mm spacing, as shown in Figure 1 c and d. Although each trace was taken as a continuous contour, a pitch of 0.1 mm was used. The circumferential spacing was selected based on being half the recommended spacing between traces when measuring wear of total hip prostheses according to ISO 14242-2 [40]. Thirty-two equally spaced vertical traces was selected as this demonstrated convergence of the calculated taper angle with that calculated using the horizontal traces.

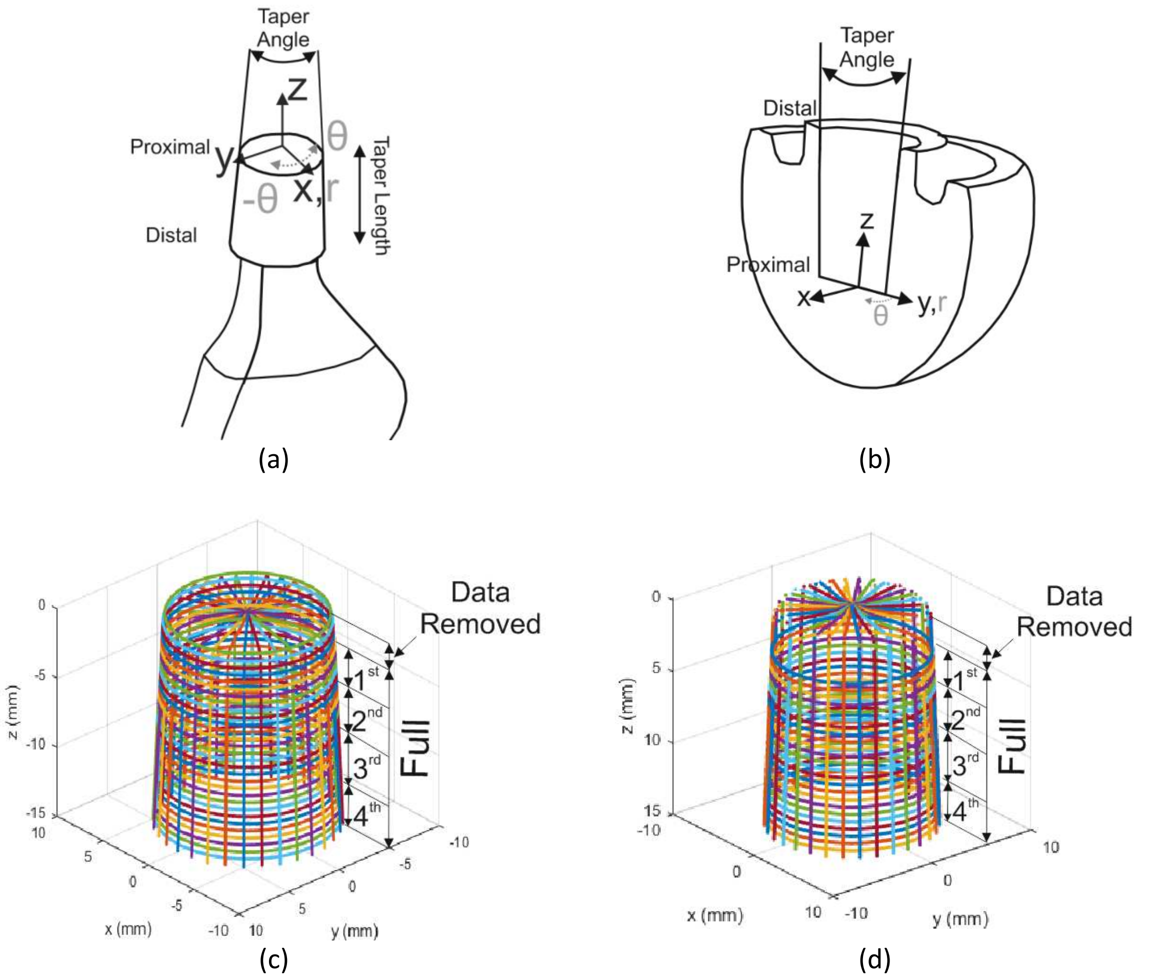

Figure 1 Schematic of the CMM cartesian (black) and cylindrical polar (grey) coordinate systems with respect to the (a) male taper stem geometry and (b) female taper head geometry. Vertical and circumferential scans on a (c) male taper and (d) female taper. Annotations indicate the data removed for analysis and the quarter cone analysis using the vertical scans (i.e. ‘1st’, ‘2nd’, ‘3rd’ and ‘4th’) and full length of the taper (i.e. ‘full’).

The raw data was exported in 3D cartesian coordinates to allow bespoke analysis using MatLab (R2017a, MathWorks, USA). Stems were aligned with the coordinate systems as shown in Figure 1a by using the symmetry of the stems in a vice and engineering parallels to minimise the amount of rotation about the z-axis between stem measurements.

Prior to any analysis, the chamfer of the male taper and the proximal clearance area of the female taper was removed from all the data sets. This was achieved by excluding data from the first 1.5 mm of the male tapers (i.e. from z = 0 to z = -1.5 mm) and the first 2 mm of the female taper (i.e. z = 0 mm to z = 2 mm, Figure 1 c and d). Taper angle (or cone angle) was then calculated independent of any rotation about the x and y axes by using two directly adjacent vertical traces and applying the cosine rule. This was done using both the full length of the taper and by segmenting it into quarters as shown in Figure 1 c and d. The first step was to apply a linear regression to each segment to find the relationship between the x, y and z coordinates. These were then used to determine the vector equation of each segment before applying the cosine rule to the directly opposite corresponding segment vector (see Figure 1 c and d). This was repeated and averaged over the sixteen different planes about the taper axis i.e. using two vertical scans located on direct opposite sides of the taper for a single plane.

Circumferential traces were used to determine deviation from the ideal cone. Tilt about the x and y axes was removed prior to analysis. This was achieved by first finding the relationship between x, y and z coordinates of the centres of each circumferential traces (Figure 2a). Two angles were then calculated from this linear relationship: 1) between the y-z plane and the component of the linear relationship in the x-z plane (α_1, Figure 2b) and 2) between the x-z plane and the component of the linear relationship in the y-z plane (α_2, Figure 2c). These angles were then used to create two rotation matrices for rotation about the y-axis ($\mathrm{T}_{\mathrm{rot\,y}(\alpha_1)}$, Equation 1) and x-axis ($\mathrm{T}_{\mathrm{rot\,x}(\alpha_2)}$, Equation 2).

$$\mathrm{T}_{\mathrm{rot\,y}(\propto_1)} = \begin{bmatrix} \cos(\alpha_1) & 0 & \sin(\alpha_1) \\ 0 & 1 & 0 \\ -\sin(\alpha_1) & 0 & \cos(\alpha_1) \end{bmatrix} \qquad \text{Equation 1}$$

$$\mathrm{T}_{\mathrm{rot\,x}(\alpha_2)} = \begin{bmatrix} 1 & 0 & 0 \\ 0 & \cos(\alpha_2) & -\sin(\alpha_2) \\ 0 & \sin(\alpha_2) & \cos(\alpha_2) \end{bmatrix} \qquad \text{Equation 2}$$

After rotating all the points from the circumferential traces it was then translated to centre all the data about the origin (Figure 2d).

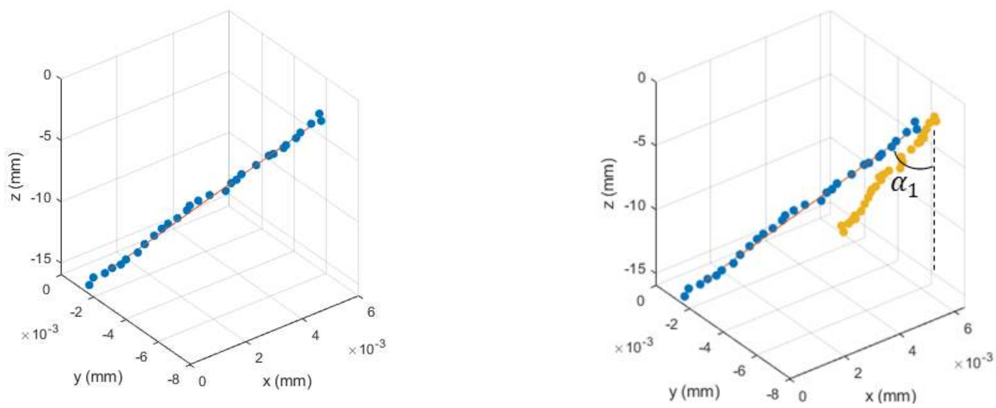

(a) (b)

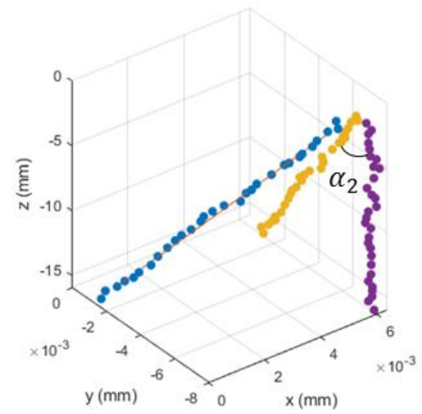

(c)

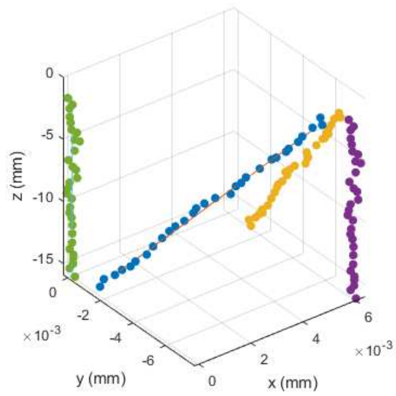

(d)

Figure 2 (a) Centres of each circumferential trace and 3D linear regression (b) rotation about the y-axis i.e. in the x-z plane (c) rotation about the x-axis i.e. in the y-z plane and (d) translation about the origin.

Ideal taper angle was calculated by converting to a cylindrical polar coordinate system (Figure 1a and b). Cone angle was determined by taking tangent of the gradient coefficient of the linear relationship between radii (r) and the z-axis. The full taper length was used as the cone generator (i.e. equation of the line of best fit that relates radius to the z position along the taper) for determining deviation from the ideal cone. Still within cylindrical polar coordinates, the ideal cone radii at any given z-value was calculated from the cone generator and taken from the radial position (r) of each point. Deviation was then plotted as a surface plot against position around the taper (θ) and the z-axis of the taper.

Taper angles and deviation from the cone was also verified with a predeveloped cone analysis software (Sphere Profiler, Redlux, UK). There was less than a 0.0001 ° discrepancy in cone angle between the bespoke MatLab analysis and the predeveloped geometry analysis software with matching deviation patterns (Figure 3).

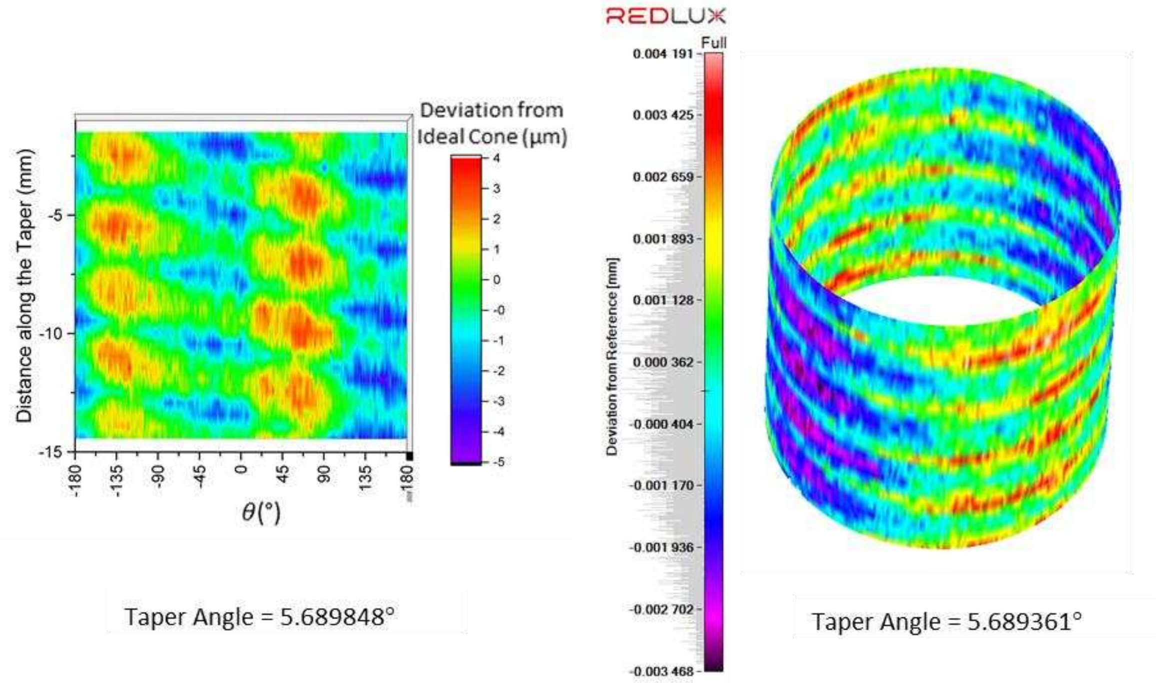

(a) (b)

Figure 3 Example of a taper analysed using the (a) bespoke MatLab programme and (b) predeveloped Redlux analysis which shows similar taper angles and deviation patterns.

2.1. Statistics

Data is presented as a mean ± 95 % confidence intervals unless stated otherwise. Taper angles were compared using 1-way analysis of variance followed by the students t-test. Level of significance was set at p-value of 0.05 for all statistical tests. The statistical analyses were performed using Excel (Microsoft, USA).

3. Results

3.1. Taper Angle

Figure 4 shows the calculated male taper angles. These varied between male tapers, even those of the apparent same type i.e. the '12/14' male tapers (P-value <0.05). Statistical difference was seen between the majority of the male tapers, including those of the same type and manufacturer e.g. MT7 and MT11 with MT12. The '12/14' male tapers demonstrated an average taper angle of 5.659 ± 0.0131 ° and range of 0.08 °, shown in Figure 4a. MT8 ('10/12' taper) and MT10 (Type 1 taper) demonstrated a significantly reduced average angle of 3.070 ° and 3.773 ° respectively (Figure 4b and c). Figure 4 displays the cone angles and confidence intervals from repeats on separate samples of the same type and the 16 different planes about the z-axis providing an indication of "roundness". The smallest confidence intervals belong to spigots (MT4 and MT5) and, MT7.

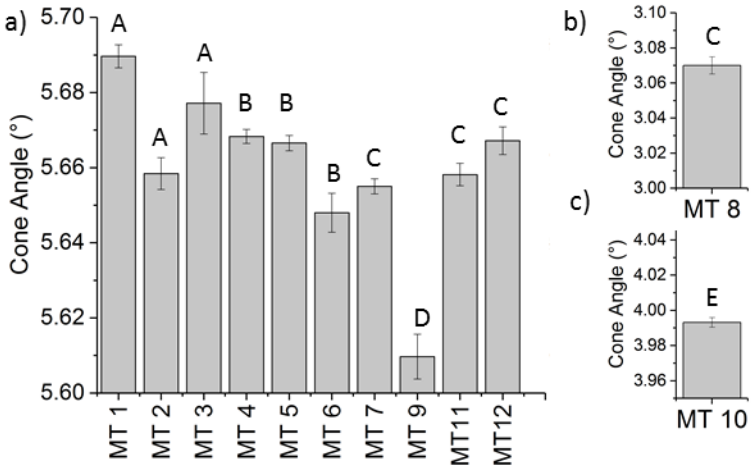

Figure 4 Taper angles of (a) '12/14' male tapers and (b) '10/12' (MT8) and (c) Type 1 (MT10). Letters above each bar indicates the manufacturer (see Table 1). Error bars correspond to the 95 % confidence intervals from the taper angles calculated using the sixteen equally spaced different cones about the z-axis. NB although the scales are very different the range are a consistent 0.1° for comparison.

The female taper angles, all of which are '12/14', were different (p-value <0.05) except FT2 and FT4 (Figure 5). The female tapers demonstrated an average larger cone angle of 5.712 ± 0.043 ° and range of 0.13 ° compared to the '12/14' male tapers, providing a predominantly proximal contact between ideal cones. However, FT5 and FT6 from manufacturer C presented a much smaller taper angle. The female tapers presented a similar taper angle variation between tapers of the same type as the male tapers reflected by the confidence intervals in Figure 4 and Figure 5.

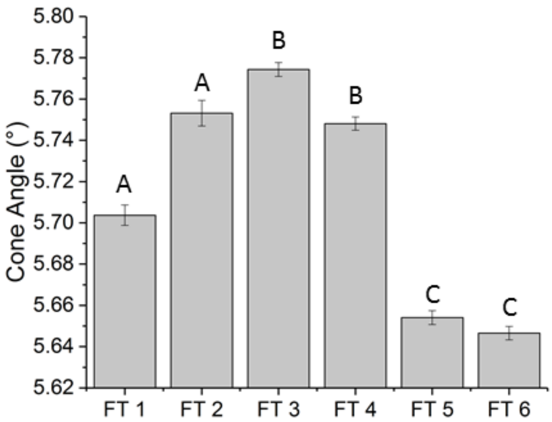

Figure 5 Taper angles of all female tapers. Letters above each bar indicates the manufacturer (see Table 1). Error bars correspond to the 95% confidence intervals from the taper angles calculated using the sixteen equally spaced different cones about the z-axis.

Variation in cone angle also occurred along the length of the taper providing an indication as to 'straightness'. Figure 6 shows cone angle calculated from the male tapers segmented into quarters. There appeared to be no consistent variation pattern between the tapers but there was statistical difference between the quarters in most of the male taper apart from MT3 and MT7. MT10 demonstrated the largest variation in cone angle down the taper with a maximum difference of 0.169 ° between the quarters. The smallest variation was seen by the MT7 with a difference of 0.003 °.

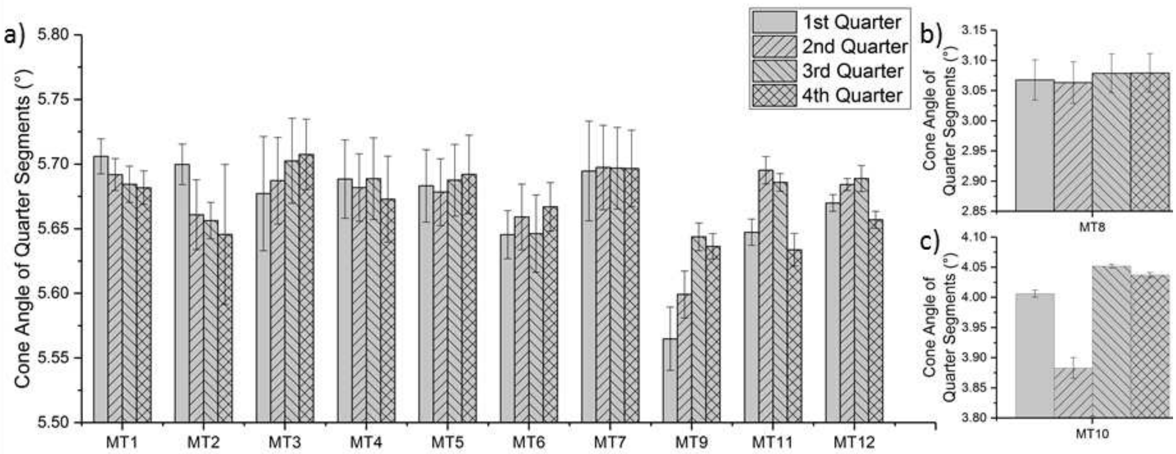

Figure 6 Male taper angles segmented into quarters where the 1st quarter corresponds to the most proximal and the 4th quarter corresponds to the most distal. (a) '12/14' male tapers and (b) the '10/12' (MT8) and (c) Type 1 taper (MT10). NB although the scales are very different the range are a consistent 0.3 ° for comparison.

Taper angle variation along the length was also seen in the female tapers, as shown in Figure 7. Similar variation in cone angle was seen in the different quarters between the male and female tapers. Variation between the quarters were all significantly different.

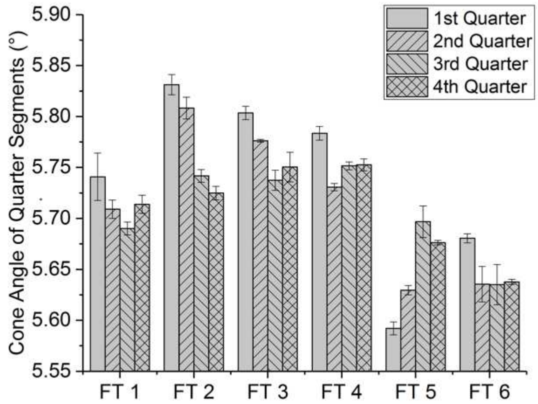

Figure 7 Female taper angles segmented into quarters where the 1st quarter corresponds to the most proximal and the 4th quarter corresponds to the most distal.

3.2. Deviation from the Ideal Cone

3.2.1. Male Tapers

The variation in taper angle around and along the z-axis of the taper (i.e. 'roundness' and 'straightness') are due to deviations from the ideal cone. Figure 8 shows surface deviation patterns for the male tapers. In cases where there was more than one sample per taper for measurement, the same deviation pattern was observed. Clear 'threaded' patterns were seen in: MT3, the spigots (MT4 and MT5), MT6, MT7 and MT12 (Figure 8a, b, c, d and e respectively). The largest pitch of 0.286 mm was measured on MT7, using simple circle geometry a pitch of 0.286 mm would allow a

1.5 mm diameter ruby a circle sagitta of 0.0136 mm. corresponding with great precision to the CMM deviation range of the ideal cone of 0.0136 mm. Out of “roundness” in the form of ovality demonstrated by a two sine waves equally distributed around the taper was seen in MT8 and MT10 (Figure 8f and g respectively). MT1, MT2 and MT11 demonstrated a deviation pattern characteristic of a ‘threaded’ taper with ovality (Figure 8h, i and j respectively). MT9 presented the smallest deviation range of 0.0035 mm (less than 40 % of the average deviation range of all the male tapers) with a pattern that indicated that there might have been ideal cone fitting mismatch (Figure 8k). The location of the major and minor axes of ovality were distributed at the same location relative to the stem geometry for the MT8, MT2 and MT11 tapers. The major axis occurred at approximately θ = 0 ° and θ = ± 180 ° (in cylindrical polar coordinates) corresponding the plane of them stem that would allow provide the smallest second moment of area as shown in Figure 1a. The collared MT1 and MT10 presented an oval pattern that was out of phase with MT2 and MT8 (both of which are non-collared) by around 60 °.

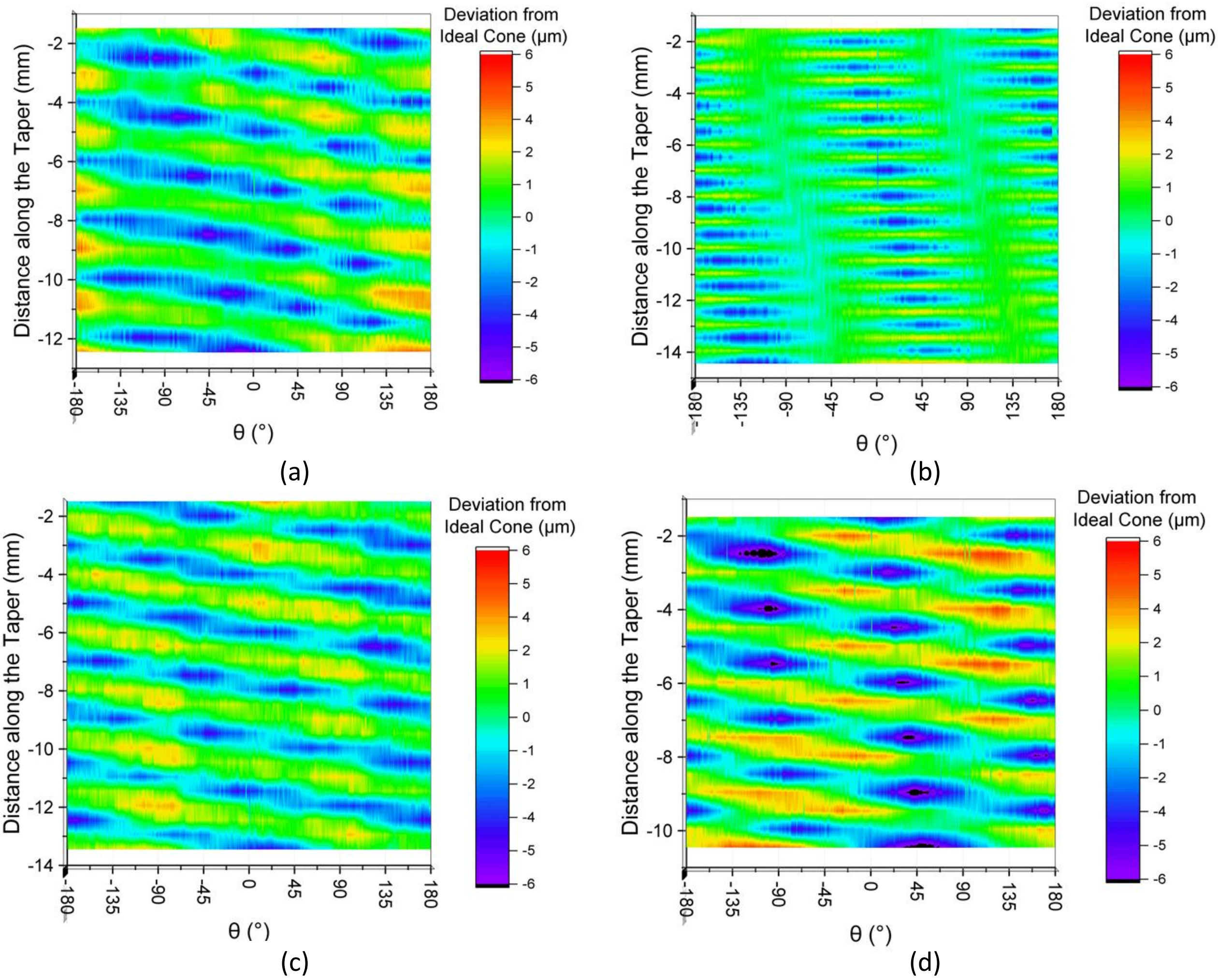

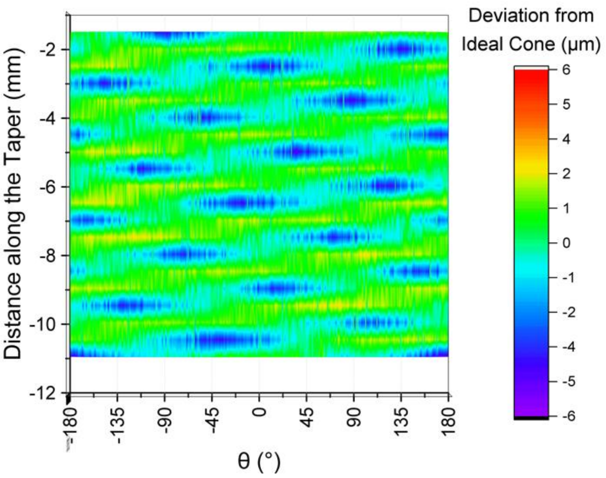
Deviation from
Ideal Cone (µm)
Distance along the Taper (mm)
θ (°)

(e)

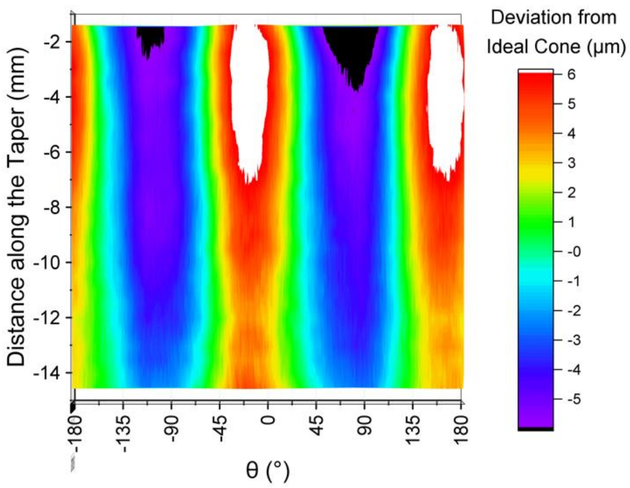
Deviation from
Ideal Cone (µm)
Distance along the Taper (mm)
θ (°)

(f)

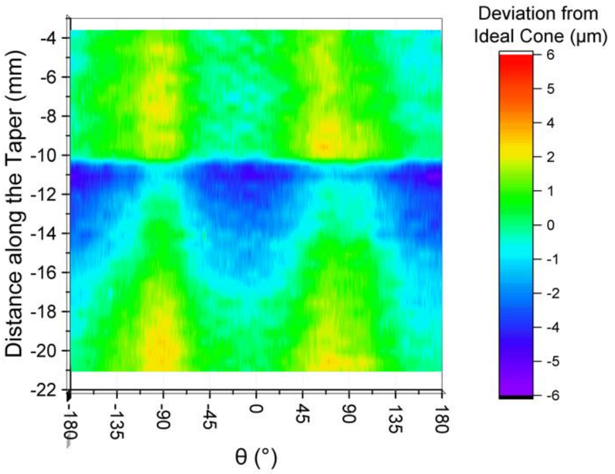
Deviation from
Ideal Cone (µm)
Distance along the Taper (mm)
θ (°)

(g)

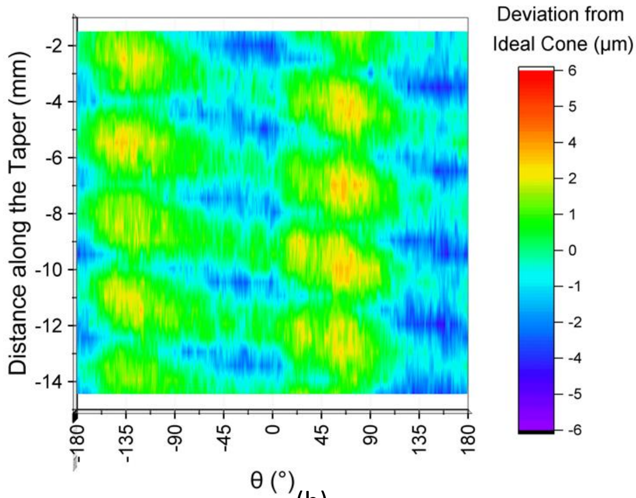
Deviation from
Ideal Cone (µm)
Distance along the Taper (mm)
θ (°)

(h)

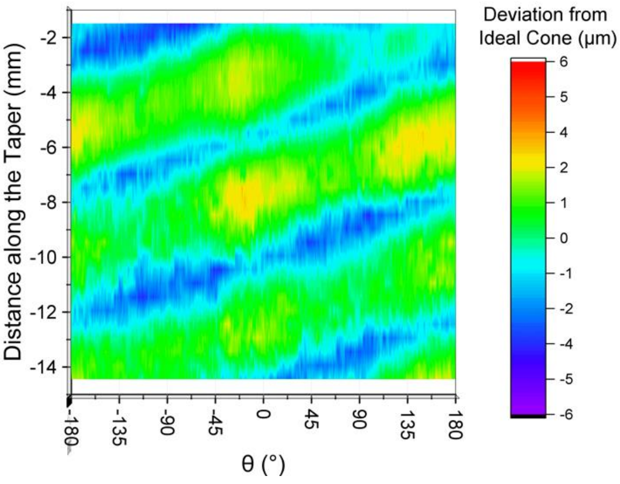
Deviation from
Ideal Cone (µm)
Distance along the Taper (mm)
θ (°)

(i)

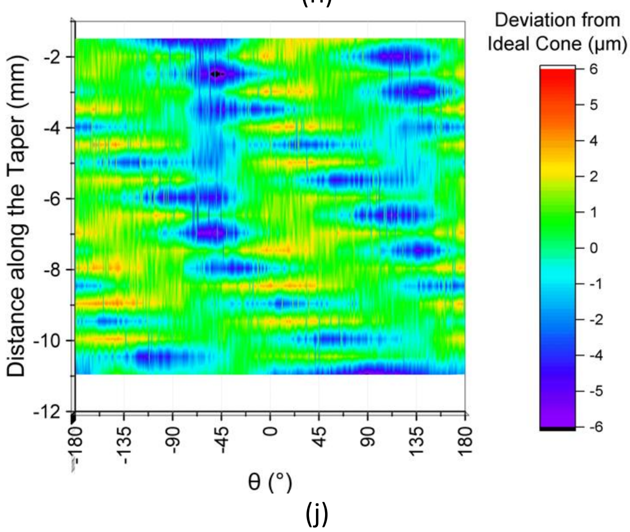
Deviation from
Ideal Cone (µm)
Distance along the Taper (mm)
θ (°)

(j)

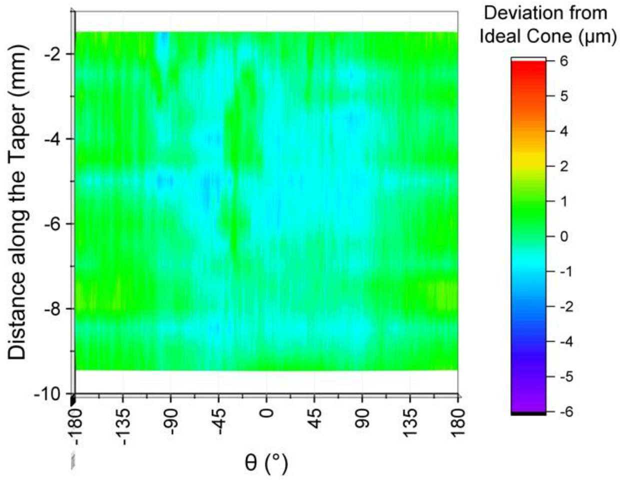

(k)

Figure 8 Surface maps of the deviation from the ideal cone in cylindrical polar coordinates for male tapers. (a) MT3 (b) MT4 (c) MT6 (d) MT7 (e) MT12 (f) MT8 (g) MT10 (h) MT1 (i) MT2 (j) MT11 (k) MT9.

3.2.2. Female Tapers

The female and male tapers presented a similar range of deviation (10 µm vs 9 µm for male and female tapers respectively) but very different deviation patterns. In cases where there was more than one sample of the same taper for measurement, the same deviation pattern was observed. Figure 9 shows the deviation maps from the ideal cone for all the female tapers. Three different patterns were observed in the female tapers. FT1 and the ceramic FT4 tapers presented no repeating patterns around the taper z-axis or along it (Figure 9a and b). No repeating patterns were presented in FT1 and FT4 indicate eccentricity that could be a function of ideal cone fitting mismatch. The ceramic taper (FT4) demonstrated the smallest deviation range, around 40 % smaller than other female tapers. The four remaining female tapers presented a third order harmonic around the z-axis of the taper including: FT2, FT3, FT 5 and FT 6 (Figure 9c, d, e and f). It was noted that the four female tapers that presented this triple harmonic belonged to all the solid metal heads in this study. FT2 was the only other CoCrMo head in this study did not present this pattern and was of a separate bearing surface and taper insert (i.e. hollow).

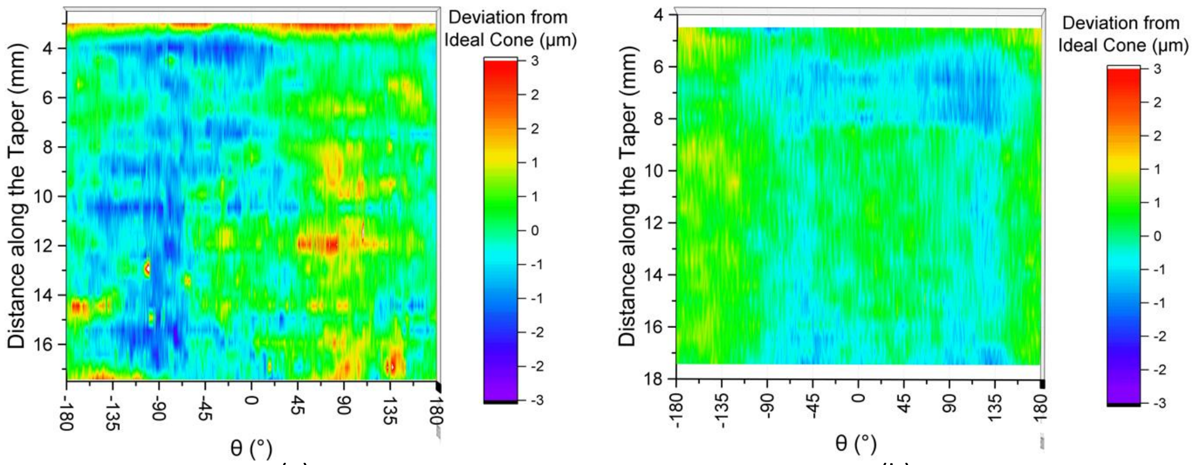

(a) (b)

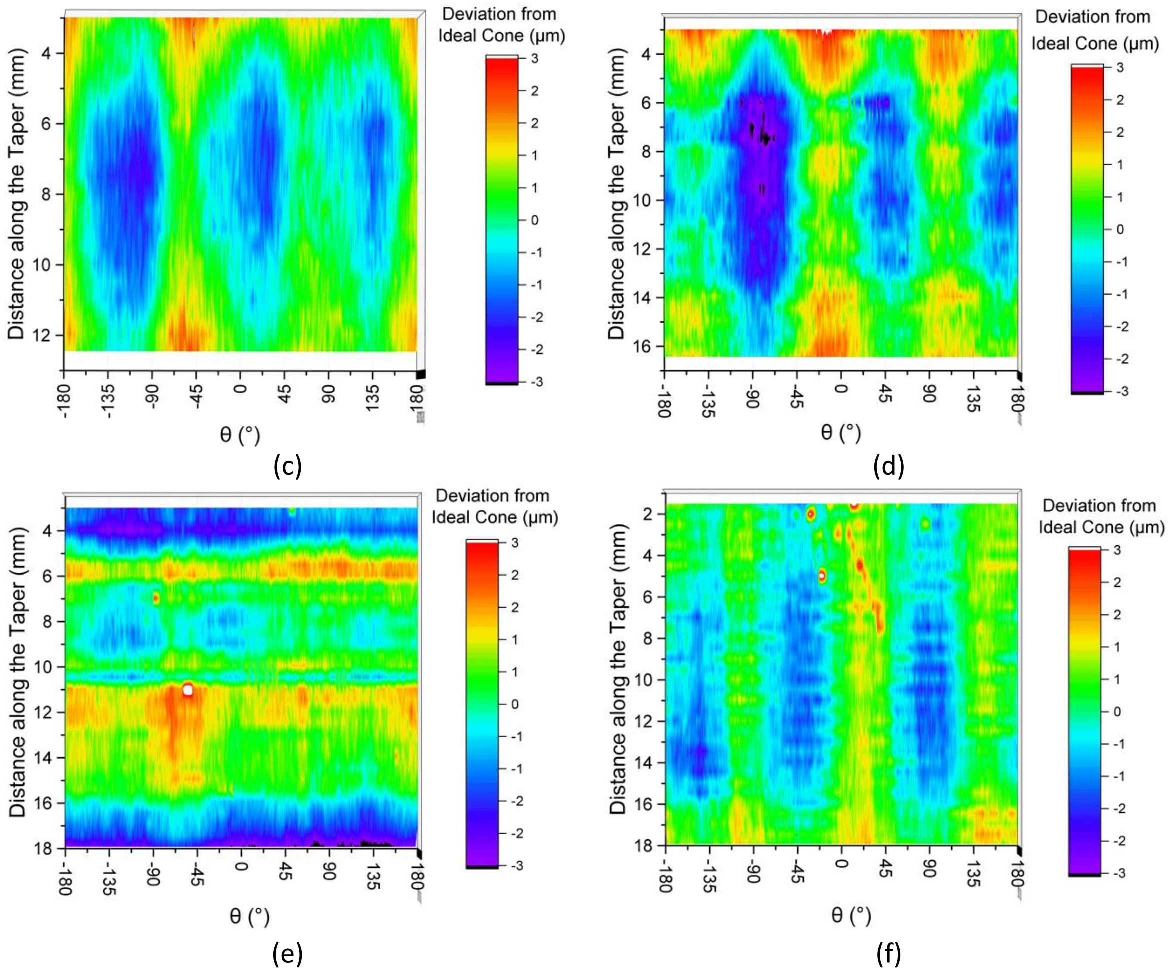

Figure 9 Surface maps of the deviation from the ideal cone in cylindrical polar coordinates for female tapers. (a) FT1, (b) FT4, (c) FT2, (d) FT3, (e) FT5 and (f) FT6.

4. Discussion

The aim of this study was to assess variations in commercially available male and female THR head and stem tapers providing a greater insight into possible engagement. The largest limitation in assessing variation across the market came from the number of repeat samples for each taper. Although an aim of a minimum of three samples per taper measured, this was not always possible. The limited number of samples should be taken into account when drawing conclusions form this study, especially where only one was available for measurement. Another limitation of this study was the use of a contacting CMM with a 1.5 mm diameter ruby tipped stylus. This introduced a degree of mechanical filtering of the surfaces which meant that finer surface topographical characteristics such as machining mark were not accurately captured.

One of the first observations of this study was that tapers of the apparent same type (i.e. '12/14') presented different ideal geometries. Variation in the '12/14' male taper cone angles varied by a range of 0.08 ° (Figure 4a). While the '12/14' female taper cone angle varied by a range of 0.13 ° (Figure 5). Both male and female cone angle variation ranges agreed with Mueller et al. [37] that reported a variation of about 0.1 ° between manufacturers. Likewise, MT10 presented a smaller cone angle than the '12/14' tapers and within the range given by Nassif et al. [41]. The '10/12' taper (MT8) presented the smallest cone angle, closer to that intended by Morse to resist shear stresses [1]. Smaller taper angles would decrease the taper locking stiffness allowing a greater displacement under the same impaction loads, increasing seating energy as explained by Ouellette et al. [42]. However, it is unclear how taper angle might affect performance of the junction under biological loading condition and if Morse's original design criteria of only a slight taper is beneficial.

Taper angle was affected by 'roundness' and 'straightness'. Variation in the cone angle within the different planes about the z-axis of the taper provided a good indication of out of 'roundness'. While differences between the cone angles once split into quarters gave an indication as to the 'straightness' of the conical tapers. This effect of 'straightness' was seen directly in The Type 1 taper (MT10) that demonstrated the largest maximum and minimum cone angles calculated from splitting the taper into quarters. This was predominantly due to variation seen in the 2nd quarter (Figure 6c), corresponding to the large step seen in the deviation from the cone maps at around z= -11 mm (Figure 8g).

Assuming an ideal geometry, deviations in 'straightness' and 'roundness' present uniquely different patterns between female and male tapers. Therefore, this study suggests that engagement of a taper junction in modular head-stem THR is not as simple as that predicted by angular mismatch of the ideal geometries. Rather, engagement or contact area is specific to a particular head-stem couple subject to differences in geometrical form with a waviness and roughness that will result in a stochastic contact. In regions of sufficient compressive stress these contacting asperities will experience deformation altering the as-manufactured surfaces [39]. Further changes to the surface will also arise from fretting-corrosion, constantly wearing and corroding the contacting asperities leading to a transient interface changing with time in situ [43]. Studies have identified that wear and corrosion at the interface is enhanced with a decrease in conformity in terms of a 'rough' male taper, shorter engagement lengths and other features that reduce conformity such as the 'scalloped' regions present in SROM stems [29,32,36]. The patterns observed in this study will have an implication on conformity at this interface and actual contact area, as was reported by Jones et al.[42] that found different contact area distributions that support the 'roundness' and 'straightness' patterns observed in this study. Future work is aimed at mapping out a link between taper design and performance in terms of this highly transient interface. This will help understand if these variations seen in this paper are significant to performance over time and ultimately to their clinical performance.

This study found that both male and female taper angles presented differences, not only between manufacturers, but between products with the same taper type and of the same manufacturer. Taper angle is arguably the most important manufacturing tolerance to ensure a tight uniform fit between male and female tapered surfaces. The most applicable standards for tolerances are detailed by ISO 1947 [44] which describes twelve different taper angle tolerance grades from AT1 to AT12. For cones of between 10-16 mm length the tightest tolerance grade (AT1) prescribes a maximum variance of 10” (0.003 °) in cone angle (AT_α, see Figure 10) and 0.4-0.6 µm between the largest and smallest diameter (AT_D) at the end of the cone (L). At the same taper length the loosest tolerance grade (AT12) prescribes maximum variances of 21’38” (0.36 °) in cone angle and 63-100 µm difference in diameter at L.

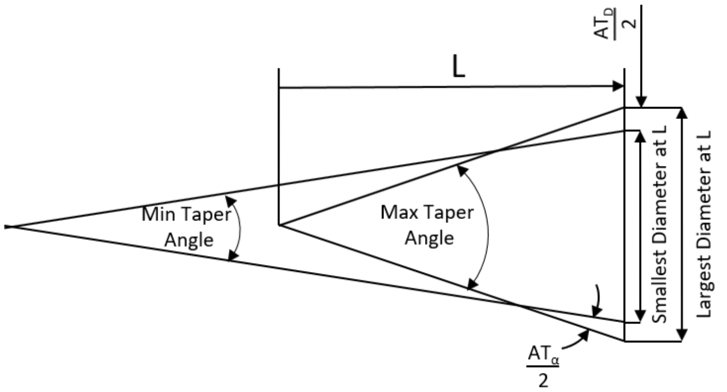

Figure 10 Schematic of the relevant taper tolerances described in ISO 1947 [44].

Most modern CNC machines have tapered interfaces that are made to AT3 or tighter for radial accuracy. For a taper of 10-16 mm length AT3 prescribes a maximum variances of 21’’ (0.006 °) cone angle and 1.0-1.6 µm difference in diameter at L. This tolerance is especially important for interfaces which undergo higher rotational speeds and greater cutting forces [45]. The tighter fit reduces vibration which has been shown to initiate fretting and affect the quality of the workpiece [45,46].

The manufacturing tolerances of taper angles in THR are not public knowledge although we can measure the range of samples used in this study. Using these and other published measurements of THR tapers we noted a maximum difference of around 0.05 ° in cone angle and 20 µm in diameter for a given taper design from the same manufacturer [37]. The diameter may also have been underestimated due to a level of mechanical filtering from the 1.5 mm ruby tipped stylus. This would place clinical tapers closer to the tolerance grade of AT8 (AT_α = 0.057°, L = 10-16 µm), if not beyond.

No manufacturing process will ever be able to produce ‘perfect’ surfaces, especially not on complex geometrical shapes such as is present in THR. However, this study does suggest that more can be done in the way of increasing conformity at the interface in THR if tapered interfaces in CNC machines can be routinely manufactured to AT3 tolerance grades or tighter. Future work that involves mapping out the link between taper design and performance is aimed at providing evidence for guidelines as to what tolerance grades are required, and a common understanding of what a ‘good’ taper interface in THR might look like.

4.1. Taper Angle Mismatch

The angular mismatch between the cones of female and male tapers (i.e. the difference in cone angle between the female and male taper) affects engagement and the contact mechanics of the taper junction [30]. Assuming there was no mixing of female and male tapers between manufacturers, the majority of possible head-stem couples presented a proximal angular mismatch (i.e. contact is predicted to be concentrated towards the inner most point of the taper junction, away from the taper opening) with an average value of 0.0231 ± 0.008 ° (Figure 11a). Proximal contacts are a design feature for ceramic head couples to ensure most of the stress is experienced by the portion of the head with the most material [1]. However, 69 % of manufacturer C head-stem couples presented a distal mismatch of -0.0125 ± 0.002 ° (i.e. contact is predicted to be concentrated towards the opening of the taper junction). In this case, male taper angles were consistent with other ‘12/14’ male tapers (MT7, Figure 4a) and female taper angles were smaller compared to other ‘12/14’ female tapers (FT5 and FT6 in Figure 5), suggesting this mismatch was governed by a smaller female taper angle. The remaining 31 % presented an average mismatch of 0.008 ± 0.002 °, possibly an attempt to achieve a matched contact for metal-on-polymer bearing couples. There was significant difference between all manufacturer mismatch angles with a p-value < 0.05 between groups.

Despite mixing head and stems from different manufacturers being discouraged and classed as ‘off-label’, one study by Tucker et al[47] reported that this does happen and resulted in a higher failure rate. Figure 11b shows the distribution of angular mismatch for matched manufacturer couples verses mixed manufacturer couples. On average the angular mismatch between the matched and mixed manufacturer couples is similar. The mixed manufacturer couples demonstrated on average a slightly larger proximal mismatch, greater distribution and range of possible angular mismatches than the matched manufacturer couples. Depending on which two manufacturers are involved in the mixed head-stem couple, angular mismatch will likely be increased but in very few cases this can be decreased.

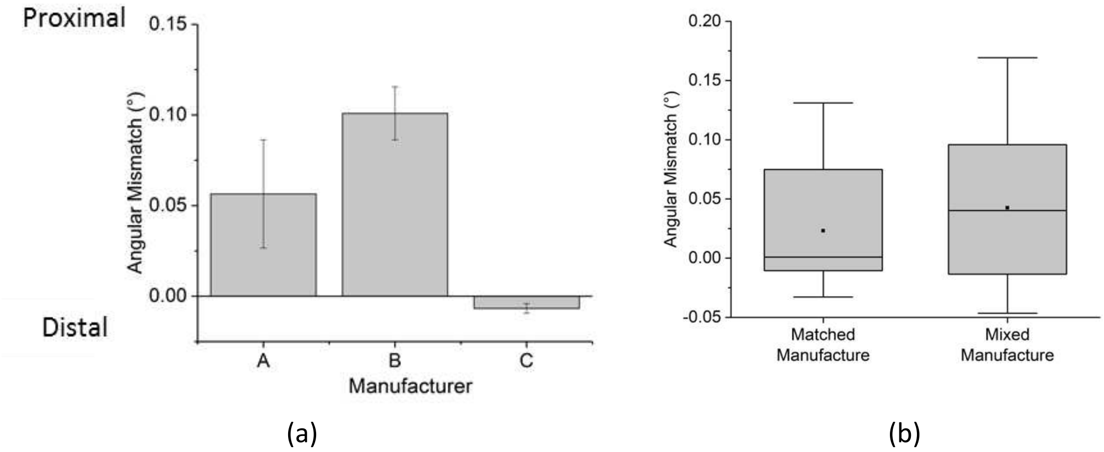

Figure 11 (a) Angular mismatch between cone angles of all matched manufacturer couples, separated by manufacturer. (b) Box plots that demonstrated the spread of angular mismatches for matched manufacturer couples vs mixed manufacturer couples (NB excluding MT8 and MT10), where the mean value has also been indicated by the block square point within each data set.

Some in-silico studies suggest that increasing conformity would reduce micro-motion at head-stem tapers and in-vitro studies at neck-stem adapters [30,48] . Where micro-motion could increase by 3 µm for every 0.1 ° of angular mismatch. In comparison, this study found a maximum proximal angular mismatch of 0.131 ° and distal mismatch of -0.024 °, suggesting an increase in micro-motion by 4 µm and 0.7 µm respectively, possibly increasing the amount degradation via fretting-corrosion. Other studies suggest that the level of angular mismatch present in the head-stem junction has an insignificant effect compared to other variables [49,50]. Therefore, small manipulations of angular mismatch at the micro scale, like increasing the distal taper junction contact could create a seal to prevent fluid ingress, reducing fretting-corrosion as suggested by Witt el al. [39]. However, it is unknown how the effect of other design parameters such as offset interact with mismatch and if this can be optimised with proximal and distal mismatches.

4.2. ‘Roundness’ and ‘Straightness’

4.2.1. Male Tapers

Deviation from the idealised male taper geometry appeared to be linked to the flexural rigidity of the taper and lower stem geometry. For example the narrowest ‘10/12’ taper (MT 8) presented the greatest out of ‘roundness’ demonstrated in Figure 8f. The pattern demonstrated noticeable ovality correlating with differences in the second moment of area of the lower stem geometry shown schematically in Figure 12 . The major axis of the oval occurred at roughly θ = 0° and θ = ±180°, which corresponds to the smaller second moment of area of the lower stem geometry. The smaller second moment of area allowing the male taper (workpiece) to flex away from the cutting tool allowing for material to lie above the ideal cone. Figure 8f also demonstrated an increase in deviation from the ideal cone towards the proximal end of the taper, consistent with simple engineering beam bending theory principles. Conversely, the spigots (MT4 and MT5) did not presented a difference in second moment of area and presented one of the smallest confidence intervals in ideal taper angle (Figure 4) and a small variation in the quarter cone angles (Figure 6), indicating good dimensional control during manufacture. MT7 presented the smallest variation in taper angle and good dimensional control as shown by the surface deviation maps (Figure 8d). MT7 also presented the shortest ideal engagement length for better control during manufacture.

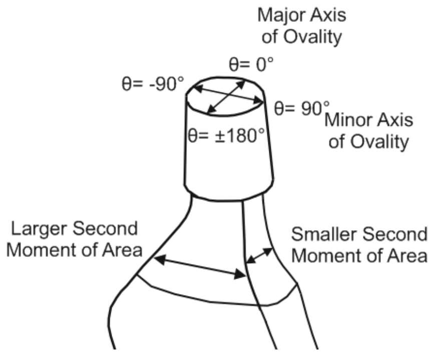

Figure 12 Schematic of how ovality relates to differences in second moments of area of the lower neck geometry.

Ovality was also seen in MT1, MT2, MT10 and MT11 (see Figure 8g, h, i and j). Where the non-collared MT2 and MT11 presented ovality where the major axes occurred at θ = 0° and θ = ±180° corresponding to the smaller second moments of area, as was with MT 8. However, the collared MT1 and MT 10 presented an oval pattern that was out of phase with the non-collared MT2, MT8 and MT11 by around 60 °. One possible explanation for this is the collar altering the second moments of area from what they would be if they were non-collared.

The elastic strain experienced during manufacturer is also controlled by the material properties of the stem. One working hypothesis was that stems made with a relatively low elastic modulus such as a titanium alloy would present greater variations in the form of out of ‘roundness’ and ‘straightness’ compared to those made of a metal with a higher elastic modulus such as CoCrMo. However, results did not consistently support this hypothesis and more measurements comparing stems with a similar geometry made of different metals with a range of elastic moduli would be needed to investigate this further.

Ovality could have significant implications on fretting-corrosion of the taper junction as it would allow for stagnation of fluid and therefore increased crevice corrosion and possibly increase micro-motion due to complex biomechanical loading [27]. The effect of ovality was investigated using finite elements models by Bitter et al [51] that demonstrated increased micro-motion, contact pressures, and wear compared to a ‘perfect’ fit. Other implications this study presented are those of volume loss calculations post in-vitro assessment or from retrievals studies. Calculating the volume of theoretical fluid that fills the space between the surface generated using the CMM surface maps and maximum ideal cone (see Figure 13) presented a range of 0.5−5 mm^3 for male tapers and 2.5−11 mm^3 for female tapers. Material loss calculations of retrieved male tapers were within the range 0−0.8 mm^3 and 0.41−25.89 mm^3 for female tapers [52]. Material loss in the Racasan et al. [52] study took into account a threaded surface and any "barrelling" or "hogging" form. However, differences in volume loss from other studies and theoretical mismatch in this study are of comparable scale. Additionally, ovality in the male tapers and the triple peak pattern within the female tapes would not be detected or taken into account on retrieval or damaged tapers.

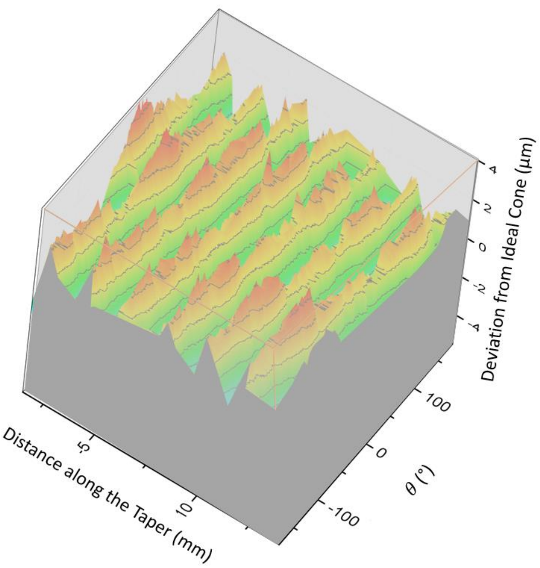

Figure 13 Schematic of theoretical volume of fluid that could fill the space between the actual taper surface and the maximum ideal cone.

4.2.2. Female Tapers

The female head tapers presented a similar level of out of roundness to the male stem tapers (see Figure 5). Although much focus has been on the topography of the male taper and whether rough or smooth male tapers have an implication on performance of the taper junction; local deviations from the ideal cone of the female taper will have just as much implications in conformity between the two components.

The four different types of female tapers that presented a third order harmonic (FT2, FT3, FT5 and FT6) were all solid metal heads while the two remaining female tapers were either a hollow metal head (i.e. assembled from a separate bearing surface and taper insert) (FT1) or ceramic (FT4). The smallest cone angle deviation range was presented by the ceramic head (FT4) corresponding to the smallest deviation range from the ideal cone possibly due to the sintering and grinding processes involved in the manufacturer of ceramic heads. Although it is not quite clear where there third order harmonic deviation pattern has come due to the spherical nature of the head, this is usually attributed to distortion of the work piece by clamping or forces experienced during manufacture [53].

5. Conclusions

Conformity and engagement between the conical surfaces in a taper junction, a key design parameter intended by Morse and is intuitively a performance determining factor. This study suggested that engagement predicted by angular mismatch of the idealised geometries may be insufficient. Rather, engagement is specific to a particular head and stem couple subject to both their micro-scale variations superimposed on their macro-scale differences across the difference length scale. Findings from this study raise the question of what a good taper junction looks like and if these junctions can be optimised for specific head-stem couples in combination with any other interacting design parameters such as offset i.e. does offset effect the performance of a distal contact the same as a distal contact? The key findings from this study include:

- Tapers of the apparent same type (i.e. '12/14') presented different geometries
- Mixing of heads and stems from different manufacturers increased the variability in angular mismatch
- Angular mismatches can be either proximal, distal or matched which could influence fretting-corrosion of different head and stem designs in different ways i.e. material couples and offsets
- Assuming an ideal geometry, deviation patterns were uniquely different between female and male tapers, and appear to be linked to the manufacturing process
- Engagement is specific to a particular head and stem couple subject to both their micro-scale variations superimposed on their macro-scale differences

6. Acknowledgments

The authors would like to thank MatOrtho LTD (UK) and the EPSRC Centre for Doctoral Training for Integrated Tribology for their support.

7. Declaration of Interest Statement

Conflicts of Interest: None

Ethical Approval: Not required

Funding: This project was funded by MatOrtho LTD (UK) and the EPSRC Centre for Doctoral Training for Integrated Tribology [Grant No. EPL01629X1].

8. References

1. Hernigou P, Queinnec S, Flouzat Lachaniette CH. One hundred and fifty years of history of the Morse taper: From Stephen A. Morse in 1864 to complications related to modularity in hip arthroplasty. *Int Orthop*. 2013;37(10):2081-2088. doi:10.1007/s00264-013-1927-0

2. Collier JP, Mayor MB, Williams IR, Surprenant VA, Surprenant HP, Currier BH. The Tradeoffs Associated With Modular Hip Prostheses. *Clin Orthop Relat Res Number*. 1995;311:91-101.

3. Traina F, De Fine M, Biondi F, Tassinari E, Galvani A, Toni A. The influence of the centre of rotation on implant survival using a modular stem hip prosthesis. *Int Orthop*. 2009;33(6):1513-1518. doi:10.1007/s00264-008-0710-0

4. Goyal N, Ho H, Fricka KB, Engh CA. Do You Have to Remove a Corroded Femoral Stem? *J Arthroplasty*. 2014;29(9):139-142. doi:10.1016/j.arth.2014.03.055

5. Garellick G, Kärrholm J, Rogmark C, Herberts P, Rolfson O. *Swedish Hip Arthroplasty Register - Annual Report 2017*.; 2017.

6. National Joint Registry for England, Wales NI and I of M. 15th Annual Report 2018. *15th Annu Rep*. 2017;1821(December 2017):218. doi:10.1038/nmat2505

7. Brown SA, Flemming CAC, Kawalec JS, et al. Fretting corrosion accelerates crevice corrosion of modular hip tapers. *J Appl Biomater*. 1995;6(1):19-26. doi:10.1002/jab.770060104

8. Gilbert JL, Buckley CA, Jacobs JJ. In vivo corrosion of modular hip prosthesis components in mixed and similar metal combinations. The effect of crevice, stress, motion, and alloy coupling. *J Biomed Mater Res*. 1993;27(12):1533-1544.

9. Goldberg JR, Gilbert JL, Jacobs JJ, Bauer TW, Paprosky W, Leurgans S. A Multicenter Retrieval Study of the Taper Interfaces of Modular Hip Prostheses. *Clin Orthop Relat Res*. 2002;401:149-161. doi:10.1097/00003086-200208000-00018

10. Cooper HJ, Della Valle CJ, Berger RA, et al. Corrosion at the head-neck taper as a cause for adverse local tissue reactions after total hip arthroplasty. *J Bone Jt Surg - Ser A*. 2012;74-A(18):1655-1661. doi:10.2106/JBJS.K.01352

11. Hall DJ, Pourzal R, Della Valle CJ, Galante JO, Jacobs JJ, Urban RM. Corrosion of Modular Junctions in Femoral and Acetabular Components for Hip Arthroplasty and Its Local and Systemic Effects. In: *Modularity and Tapers in Total Joint Replacement Devices*. 100 Barr Harbor Drive, PO Box C700, West Conshohocken, PA 19428-2959: ASTM International; 2015:410-427. doi:10.1520/STP159120140134

12. Jennings JM, Dennis DA, Yang CC. Corrosion of the Head-neck Junction After Total Hip. *J Am Acad Orthop Surg*. 2016;24(6):349-356. doi:10.5435/JAAOS-D-15-00111

13. Lindgren JU, Brismar BH, Wikstrom AC, Professor A. Adverse reaction to metal release from a modular metal-on-polyethylene hip prosthesis. *J Bone Jt Surg Br*. 2011;9393(10):1427-1430. doi:10.1302/0301-620X.93B10

14. Borden R, Pour AE, Murayama T, Blaha JD. Patient Outcomes Following Implantation of Modular Neck Hip Prostheses in Primary Total Hip Arthroplasty. In: *Modularity and Tapers in Total Joint Replacement Devices*. 100 Barr Harbor Drive, PO Box C700, West Conshohocken, PA 19428-2959: ASTM International; 2015:17-25. doi:10.1520/STP159120140151

15. Morlock M, Bünte D, Gührs J, Bishop N. Corrosion of the Head-Stem Taper Junction—Are We on the Verge of an Epidemic?: Review Article. *HSS J*. 2017;13:42-49. doi:10.1007/s11420-016-9526-4

16. Waterson HB, Whitehouse MR, Greidanus N V., Garbuz DS, Masri BA, Duncan CP. Revision for adverse local tissue reaction following metal-on-polyethylene total hip arthroplasty is associated with a high risk of early major complications. *Bone Joint J*. 2018;100-B(6):720-724. doi:10.1302/0301-620X.100B6.BJJ-2017-1466.R1

17. Morlock MM. The Taper Disaster - How Could it Happen? *HIP Int*. 2015;25(4):339-346. doi:10.5301/hipint.5000269

18. Ridon PE, Putman S, Migaud H, Berton C, Pasquier G, Girard J. Long-term comparative study of large-diameter metal-on-metal bearings: Resurfacing versus total arthroplasty with large-diameter Durom^{TM} bearing. *Orthop Traumatol Surg Res*. 2019. doi:10.1016/j.otsr.2019.04.006

19. Higgs GB, MacDonald DW, Gilbert JL, et al. Does Taper Size Have an Effect on Taper Damage in Retrieved Metal-on-Polyethylene Total Hip Devices? *J Arthroplasty*. 2016;31(9):277-281. doi:10.1016/j.arth.2016.06.053

20. Bhalekar RM, Smith SL, Joyce TJ. Wear at the taper-trunnion junction of contemporary ceramic-on-ceramic hips shown in a multistation hip simulator. *J Biomed Mater Res - Part B Appl Biomater*. 2018;(November 2017):1-11. doi:10.1002/jbm.b.34213

21. Perrigo OE. *Modern American Lathe Practice*. New York: The Norman W. Henley Publishing Co.; 1907.

22. Colvin FH. *Turning and Boring Tapers*. New York: The Derry-Collard Company; 1903.

23. BSI, ISO. BS 4500 Limits and Fits: Part 5. Specification for system of cone tolerances for conical work pieces from C=1:3 to 1:500 and lengths from 6mm to 630mm. 1988.

24. Werner PH, Etema HB, Wit F, Morlock MM, Verheyen CCPM. Basic principles and uniform terminology for the head-neck juncton in hip replacement. *HIP Int*. 2015;25(2):115-119. doi:10.5301/hipint.5000204

25. Bergmann G, Graichen F, Rohlmann A, et al. Realistic loads for testing hip implants. *Biomed Mater Eng*. 2010;20:65-75. doi:10.3233/BME-2010-0616

26. Bishop NE, Hothan A, Morlock MM. High friction moments in large hard-on-hard hip replacement bearings in conditions of poor lubrication. *J Orthop Res*. 2013;31(5):807-813. doi:10.1002/jor.22255

27. Gilbert JL, Mali SA, Sivan S. Corrosion of Modular Tapers in Total Joint Replacements: A Critical Assessment of Design, Materials, Surface Structure, Mechanics, Electrochemistry, and Biology. In: *Modularity and Tapers in Total Joint Replacement Devices*. 100 Barr Harbor Drive, PO Box C700, West Conshohocken, PA 19428-2959: ASTM International; 2015:192-223. doi:10.1520/STP159120140135

28. Hothi HS, Eskelinen AP, Berber R, et al. Factors Associated With Trunnionosis in the Metal-on-Metal Pinnacle Hip. *J Arthroplasty*. 2017;32(1):286-290. doi:10.1016/j.arth.2016.06.038

29. Whittaker RK, Hothi HS, Eskelinen A, Blunn GW, Skinner JA, Hart AJ. Variation in taper surface roughness for a single design effects the wear rate in total hip arthroplasty. *J Orthop Res*. 2017;35:1784-1792. doi:10.1002/jor.23456

30. Donaldson FE, Coburn JC, Siegel KL. Total hip arthroplasty head-neck contact mechanics: A stochastic investigation of key parameters. *J Biomech*. 2014;47:1634-16-41. doi:10.1016/j.jbiomech.2014.02.035

31. Panagiotidou A, Meswania J, Hua J, Muirhead-Allwood S, Hart A, Blunn G. Enhanced wear and corrosion in modular tapers in total hip replacement is associated with the contact area and surface topography. *J Orthop Res*. 2013;31(12):2032-2039. doi:10.1002/jor.22461

32. Brock TM, Sidaginamale R, Rushton S, et al. Shorter, rough trunnion surfaces are associated with higher taper wear rates than longer, smooth trunnion surfaces in a contemporary large head metal-on-metal total hip arthroplasty system. *J Orthop Res*. 2015;33(12):1868-1874.

doi:10.1002/jor.22970

33. Kao YYJ, Koch CN, Wright TM, Padgett DE. Flexural Rigidity, Taper Angle, and Contact Length Affect Fretting of the Femoral Stem Trunnion in Total Hip Arthroplasty. *J Arthroplasty*. 2016;31(9):254-258. doi:10.1016/j.arth.2016.02.079

34. Jauch-Matt SY, Miles AW, Gill HS. Effect of trunnion roughness and length on the modular taper junction strength under typical intraoperative assembly forces. *Med Eng Phys*. 2017;39:94-101. doi:10.1016/j.medengphy.2016.11.001

35. Woon CY, Wach A, Wright TM, Padgett DE. Taper Design, Head Material, and Manufacturer Affect the Onset of Fretting Under Simulated Corrosion Conditions. *J Arthroplasty*. November 2019. doi:10.1016/j.arth.2019.11.005

36. Hothi HS, Whittaker RK, Meswania JM, Blunn GW, Skinner JA, Hart AJ. Influence of stem type on material loss at the metal-on-metal pinnacle taper junction. *Proc Inst Mech Eng Part H J Eng Med*. 2015;229(1):91-97. doi:10.1177/0954411914567931

37. Mueller U, Braun S, Schroeder S, Sonntag R, Kretzer JP. Same Same but Different? 12/14 Stem and Head Tapers in Total Hip Arthroplasty. *J Arthroplasty*. 2017;32:3191-3199. doi:10.1016/j.arth.2017.04.027

38. Munir S, Walter WL, Walsh WR. Variations in the trunnion surface topography between different commercially available hip replacement stems. *J Orthop Res*. 2015;33(1):98-105. doi:10.1002/jor.22741

39. Witt F, Gührs J, Morlock MM, Bishop NE. Quantification of the contact area at the head-stem taper interface of modular hip prostheses. *PLoS One*. 2015;10(8):1-15. doi:10.1371/journal.pone.0135517

40. BSI. ISO 14242-2 Implants for surgery - Wear of total hip joint prostheses - Part 2 : Methods of measurement. *BSI*. 2000;14242(2).

41. Nassif NA, Nawabi DH, Stoner K, Elpers M, Wright T, Padgett DE. Taper Design Affects Failure of Large-head Metal-on-metal Total Hip Replacements. *Clin Orthop Relat Res*. 2014;472(2):564-571. doi:10.1007/s11999-013-3115-3

42. Ouellette ES, Shenoy AA, Gilbert JL. The seating mechanics of head-neck modular tapers in vitro: Load-displacement measurements, moisture, and rate effects. *J Orthop Res*. 2018;36(4):1164-1172. doi:10.1002/jor.23725

43. Morlock MM, Dickinson EC, Günther KP, Bünte D, Polster V. Head Taper Corrosion Causing Head Bottoming Out and Consecutive Gross Stem Taper Failure in Total Hip Arthroplasty. *J Arthroplasty*. 2018;33(11):3581-3590. doi:10.1016/j.arth.2018.07.017

44. ISO1947-1973. BS 4500 Limits and Fits: Part 5. Specification for system of cone tolerances for conical work pieces from C=1:3 to 1:500 and lengths from 6mm to 630mm. 1988.

45. David A. Stephenson JSA. Toolholders and Workholders. In: *Metal Cutting Theory and Practice*. 3rd ed. New York: Taylor & Francis Group; 2016:280-332.

46. Rivin EI. Advanced 7/24 taper toolholder/spindle interfaces for high-speed CNC machine tools. *SAE Tech Pap*. 1998;(724). doi:10.4271/981866

47. Tucker K, Pickford M, Newell C, Howard P, Hunt LP, Blom AW. Mixing of components from different manufacturers in total hip arthroplasty: Prevalence and comparative outcomes. *Acta Orthop*. 2015;86(6):671-677. doi:10.3109/17453674.2015.1074483

48. Haschke H, Jauch-Matt SY, Sellenschloh K, Huber G, Morlock MM. Assembly force and taper angle difference influence the relative motion at the stem-neck interface of bi-modular hip prostheses. *Proc Inst Mech Eng Part H J Eng Med*. 2016;230(7):690-699. doi:10.1177/0954411916648717

49. Kocagöz SB, Underwood RJ, Sivan S, et al. Does taper angle clearance influence fretting and corrosion damage at the head-stem interface? A matched cohort retrieval study. *Semin Arthroplasty*. 2013;24(4):246-254. doi:10.1053/j.sart.2014.01.002

50. Ouellette ES, Mali SA, Kim J, Grostefon J, Gilbert JL. Design, Material, and Seating Load Effects on In Vitro Fretting Corrosion Performance of Modular Head-Neck Tapers. *J Arthroplasty*. 2019;34(5):991-1002. doi:10.1016/j.arth.2019.01.043

51. Bitter T, Khan I, Marriott T, Lovelady E, Verdonschot N, Janssen D. The effects of manufacturing tolerances and assembly force on the volumetric wear at the taper junction in modular total hip arthroplasty. *Comput Methods Biomech Biomed Engin*. 2019;22(13):1061-1072. doi:10.1080/10255842.2019.1627524

52. Racasan R, Bills P, Blunt L, Hart A, Skinner J. Method for Characterization of Material Loss from Modular Head-Stem Taper Surfaces of Hip Replacement Devices. In: *Modularity and Tapers in Total Joint Replacement Devices*. 100 Barr Harbor Drive, PO Box C700, West Conshohocken, PA 19428-2959: ASTM International; 2015:132-146. doi:10.1520/STP159120140139

53. Taylor Hobson. *A Guide to Roundness and Surface Texture - Measurement and Parameters*. 1st ed. Leicester: Taylor Hobson; 2017. www.taylor-hobson.com.